COMMUNICATIONS IN COMPUTATIONAL PHYSICS
Vol. **3**, No. 3, pp. 641-658

Commun. Comput. Phys.
March 2008

An Exact Absorbing Boundary Condition for the Schrödinger Equation With Sinusoidal Potentials at Infinity

Chunxiong Zheng*

Department of Mathematical Sciences, Tsinghua University, Beijing 100084, China.

Received 9 April 2007; Accepted (in revised version) 2 June 2007

Available online 30 October 2007

Abstract. In this paper we study numerical issues related to the Schrödinger equation with sinusoidal potentials at infinity. An exact absorbing boundary condition in a form of Dirichlet-to-Neumann mapping is derived. This boundary condition is based on an analytical expression of the logarithmic derivative of the Floquet solution to Mathieu's equation, which is completely new to the author's knowledge. The implementation of this exact boundary condition is discussed, and a fast evaluation method is used to reduce the computation burden arising from the involved half-order derivative operator. Some numerical tests are given to show the performance of the proposed absorbing boundary conditions.

AMS subject classifications: 65M99, 81-08

Key words: Absorbing boundary condition, sinusoidal potential, Schrödinger equation, unbounded domain.

1 Introduction

Wave propagation is usually modeled by partial differential equations on unbounded domains. For a practical numerical treatment, however, the equations need to be confined to a bounded computational domain in a neighborhood of the region of physical interest. This can be achieved by introducing artificial boundaries, which then necessitates imposing boundary conditions. The ideal boundary conditions should not only present well-posed problems, but also mimic the perfect absorption of waves traveling out of the computational domain through the artificial boundaries. Right in this context, these boundary conditions are usually called absorbing (or transparent, non-reflecting in the same spirit) in the literature.

*Corresponding author. *Email address:* czheng@math.tsinghua.edu.cn (C. Zheng)

Absorbing boundary condition for the Schrödinger equation and related problems has been a hot research topic for many years. From one-dimensional [2, 3, 6, 7, 10, 12, 15, 19–22, 24, 26] to high-dimensional [5, 8, 11, 13, 18, 23, 28], from linear to nonlinear [4, 14, 25, 27, 29], many developments have been made on the designing and implementing of various absorbing boundary conditions. In this paper we will consider the Schrödinger equation of the form

$$iu_t + u_{xx} = V(x)u, \quad x \in \mathbf{R}, \tag{1.1}$$

$$u(x,0) = u_0(x), \quad x \in \mathbf{R}, \tag{1.2}$$

$$u(x,t) \to 0, \quad x \to \pm\infty. \tag{1.3}$$

The initial function u_0 is assumed to be compactly supported in an interval $[x_L, x_R]$, with $x_L < x_R$, and the real potential function V is supposed to be sinusoidal on $(-\infty, x_L]$ and $[x_R, +\infty)$. More precisely, we assume

$$V(x) = V_L + 2q_L \cos\frac{2\pi(x_L - x)}{S_L}, \quad \forall x \in (-\infty, x_L],$$

$$V(x) = V_R + 2q_R \cos\frac{2\pi(x - x_R)}{S_R}, \quad \forall x \in [x_R, +\infty),$$

where S_L and S_R are the periods, V_L and V_R are the average potentials, and the non-negative numbers q_L and q_R relate to the amplitudes of sinusoidal part of the potential function V on $(-\infty, x_L]$ and $[x_R, +\infty)$, respectively.

The Schrödinger equation with periodic potentials has wide applications in quantum mechanics and solid physics. For example, it can be used to model electrons immersed in optical lattices, or simulate quantum dots embedded in crystals. The problem (1.1)-(1.3) is linear, and the tool of Laplace transform is thus applicable. Formally an exact relation can be built at each boundary point. This relation expresses a convolution, with its kernel defined by the inverse Laplace transform of the logarithmic derivative of the Floquet solution to Mathieu's equation. However, if the property of this kernel is not fully explored, this formal exact relation has little practical use. Recently, Galicher [16] considered the same problem but with a general periodic potential. Formally he set up at each artificial boundary point an exact Dirichlet-to-Dirichlet mapping, which is nonlocal in both time and space.

The organization of the rest is as follows. In Section 2, we conjecture an elegant analytical expression of the logarithmic derivative of the Floquet solution. Based on this expression, an exact absorbing boundary condition in a form of Dirichlet-to-Neumann mapping is presented in Section 3. The related numerical issues are discussed in Section 4. A fast evaluation method is employed to reduce the computation burden arising from the convolution operations. Some numerical tests are given in Section 5 to demonstrate the performance of our absorbing boundary condition. The results show that highly accurate numerical solutions can be computed. We conclude this paper in Section 6.

2 A conjecture related to Mathieu's equation

The canonical form of Mathieu's equation reads

$$y''+(z-2q\cos 2x)y=0, \tag{2.1}$$

where q is a nonnegative real number. Let us first consider the characteristic value problem: Find $\lambda\in\mathbf{R}$ and $y\in C^2[0,2\pi]$, such that

$$y''+(\lambda-2q\cos 2x)y=0, \quad x\in[0,2\pi], \tag{2.2}$$
$$y(0)=y(2\pi), \quad y'(0)=y'(2\pi). \tag{2.3}$$

It is known that for a fixed $q>0$, there are a series of characteristic values $a_r(q)$ and $b_r(q)$, real, distinct and satisfying

$$a_0(q)<b_1(q)<a_1(q)<b_2(q)<a_2(q)<\cdots.$$

The characteristic function associated with $a_r(q)$ is an even function $ce_r(x,q)$, while that with $b_r(q)$ is an odd function $se_r(x,q)$. For q relatively small, the power series approximations for $a_r(q)$, $b_r(q)$, $ce_r(x,q)$ and $se_r(x,q)$ can be found in [1, p. 724].

Mathieu's equation can be transformed into a first-order ODE system

$$\begin{pmatrix} y \\ y' \end{pmatrix}' = \begin{pmatrix} 0 & 1 \\ 2q\cos 2x-z & 0 \end{pmatrix}\begin{pmatrix} y \\ y' \end{pmatrix}. \tag{2.4}$$

It has two linearly independent fundamental solutions $y_1(x)$ and $y_2(x)$ which satisfy the following initial conditions,

$$y_1(0)=1, \quad y_1'(0)=0,$$
$$y_2(0)=0, \quad y_2'(0)=1.$$

Let us set

$$A=\begin{pmatrix} y_1(\pi) & y_2(\pi) \\ y_1'(\pi) & y_2'(\pi) \end{pmatrix}.$$

For any z with $\Im z>0$, the matrix A has two characteristic values $e^{\mu\pi}$ and $e^{-\mu\pi}$, with $\Re\mu<0$. Suppose $(c,d)^T$ is a characteristic vector associated with $e^{\mu\pi}$. Then the solution $y(x)$ of (2.4) with the initial conditions

$$y(0)=c, \quad y'(0)=d, \tag{2.5}$$

satisfies $y(\pi)=ce^{\mu\pi}$ and $y'(\pi)=de^{\mu\pi}$. As a matter of fact, $y(x)$, denoted by $F(x,z,q)$ in the following, is one of the Floquet solutions in a form of

$$y(x)=e^{\mu x}\phi(x),$$

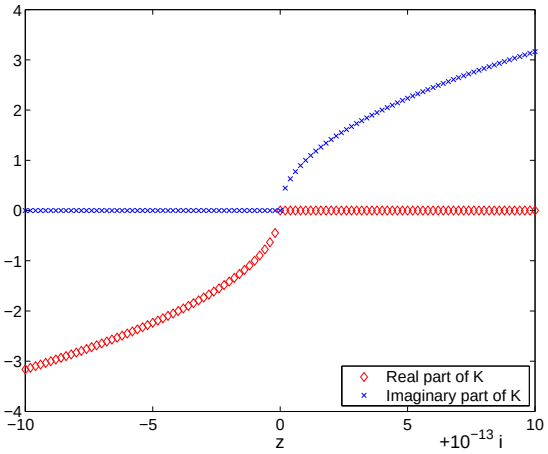

Figure 1: Plot of the computed $K(z,0)$.

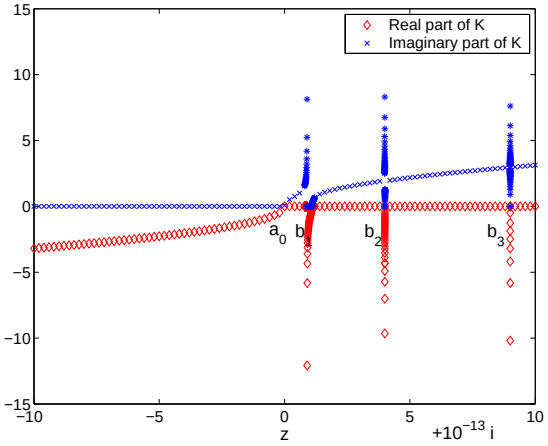

Figure 2: Plot of the computed $K(z,0.1)$.

where ϕ is a π-periodic function and μ is the periodicity exponent. See [9, p. 29] for more detail. Another Floquet solution is $F(-x,z,q)$. Thus the general solution of (2.1) with $\Im z>0$ is

$$y(x)=AF(x,z,q)+BF(-x,z,q).$$

Note that $F(x,z,q)$ is bounded on $[0,+\infty)$, while $F(-x,z,q)$ is not.

In this paper, what we are really concerned with is not the Floquet solution F itself, but its logarithmic derivative at $x=0$, i.e.,

$$K(z,q)\overset{def}{=}\frac{F_x(0,z,q)}{F(0,z,q)}.$$

For $q=0$, the Floquet solution is

$$F(x,z,0)=e^{-\sqrt{-z}x},\quad \Im z>0. \tag{2.6}$$

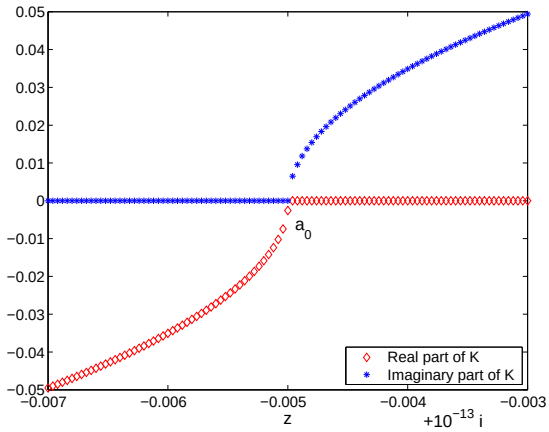

Figure 3: Plot of the computed $K(z,0.1)$.

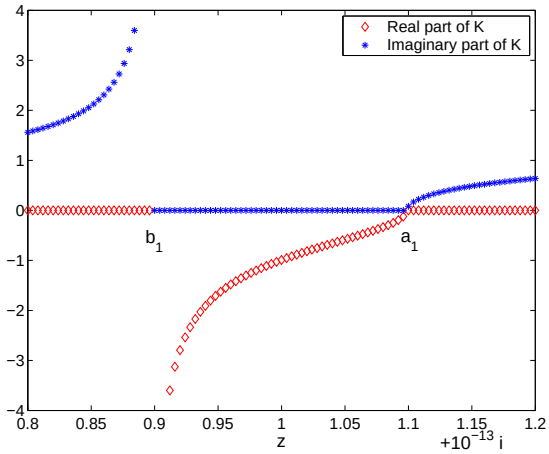

Figure 4: Plot of the computed $K(z,0.1)$.

Consequently,

$$K(z,0)=-\sqrt{-z},\quad \Im z>0. \tag{2.7}$$

But for $q>0$, to the author's knowledge, there are no such simple analytical expressions like (2.6) and (2.7) for $F(x,z,q)$ and $K(z,q)$. Fortunately, in view of (2.5) we know $K(z,q)=d/c$. Thus K at least can be evaluated numerically. The algorithm used in this paper comprises two steps:

Step 1: compute the matrix A by integrating the ODE system (2.4) with the A-stable 2-stage 4-order implicit Runge-Kutta scheme (200 time steps);

Step 2: compute the characteristic values σ_1, σ_2 with $|\sigma_1|<1<|\sigma_2|$, derive the characteristic vector $(c,d)^T$ associated with σ_1, and set $K(z,q)=d/c$.

In Fig. 1, we depict the numerical value of $K(z,0)$ with the above algorithm on the interval $[-10,10]+10^{-13}i$. The maximal error on 4001 equidistant grid points is less than $4.22\times$

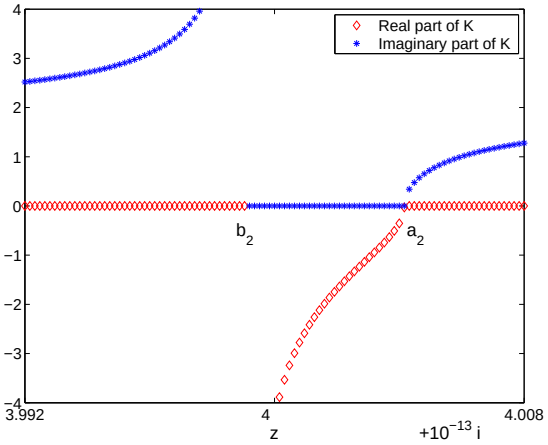

Figure 5: Plot of the computed $K(z,0.1)$.

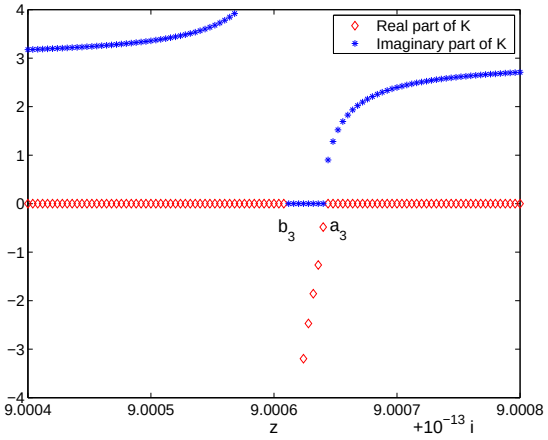

Figure 6: Plot of the computed $K(z,0.1)$.

10^{-7}, which is further reduced to 9.83×10^{-15} if the interval is changed to $[-10,10]+i$. These evidences prove the accuracy of our numerical algorithm.

Now we use our numerical algorithm to study the property of $K(z,q)$. Let $q=0.1$. Fig. 2 shows the computed $K(z,q)$ on $[-10,10]+10^{-13}i$. We can see that in addition to a non-smooth turning point a_0, there also exists three almost singular points b_1, b_2 and b_3. A closer observation (see Figs. 3 to 6) reveals that corresponding to each singular point b_r there is another non-smooth turning point a_r, and the distance between a_r and b_r becomes smaller as r changes from 1 to 3. Our numerical tests demonstrate that a_r is in fact numerically equal to $a_r(q)$ for $r=0,1,2,3$, and b_r to $b_r(q)$ for $r=1,2,3$, where $a_r(q)$ and $b_i(q)$ are the characteristic values of the problem (2.2)-(2.3). Moreover, by data fitting we find that the singularity of K at b_r behaves like $\mathcal{O}(1/\sqrt{-z+b_r})$, and the smoothness of K

at a_r seems like $\mathcal{O}(\sqrt{-z+a_r})$. Since

$$a_r(q)=r^2+o(q),\quad b_r(q)=r^2+o(q),$$

and zero potential can be taken as the limit of sinusoidal potential as $q\to 0$, we boldly conjecture that

$$K(z,q)=-\sqrt{-z+a_0(q)}\prod_{r=1}^{+\infty}\frac{\sqrt{-z+a_r(q)}}{\sqrt{-z+b_r(q)}},\quad \Im z>0,\ q\geq 0. \tag{2.8}$$

Though we cannot prove the relation (2.8) in a rigorous mathematical way, our numerical tests strongly support its validity. For example, by setting

$$K_N(z,q)\overset{def}{=}-\sqrt{-z+a_0(q)}\prod_{r=1}^{N}\frac{\sqrt{-z+a_r(q)}}{\sqrt{-z+b_r(q)}},\quad \Im z>0,\ q\geq 0, \tag{2.9}$$

in the interval $[-10,10]+10^{-13}i$, the maximal error between K_2 and K at 4001 equidistant grid points is less than 7.5×10^{-2}, and the maximal error between K_3 and K is less than 7.4×10^{-6}. Now change the interval to $[-10,10]+i$. The error between K_2 and K at 4001 equidistant grid points is less than 4.7×10^{-5}, the error between K_3 and K less than 2.2×10^{-8}, and the error between K_4 and K less than 1.8×10^{-9}. Other tests with different q have also been carried out, and all the results support our conjecture. We should remark that there is a subroutine in the FORTRAN code library IMSL which computes $a_r(q)$ and $b_r(q)$ for any $q\geq 0$.

3 An exact absorbing boundary condition

Considering the symmetry of the problem (1.1)-(1.3), we need only study how to design absorbing boundary condition at the right boundary point x_R. With our assumption, the initial function u_0 vanishes on $[x_R,+\infty)$. Doing the Laplace transform on both sides of (1.1) we get the Mathieu equation

$$\hat{u}_{xx}+\left(is-V_R-2q_R\cos\frac{2\pi(x-x_R)}{S_R}\right)\hat{u}=0,\quad x\in[x_R,+\infty), \tag{3.1}$$

where $\hat{u}=\mathcal{L}(u)$, and s is the dual variable of t. Subject to the boundary condition at infinity (1.3), for any given s with $\Re s>0$, we have $\Im(is-V_R)>0$ and the solution of (3.1) is thus

$$\hat{u}(x,s)=AF\left(\frac{\pi(x-x_R)}{S_R},\frac{S_R^2(is-V_R)}{\pi^2},\frac{S_R^2q_R}{\pi^2}\right),\quad x\in[x_R,+\infty), \tag{3.2}$$

where A is independent of x, and F is the Floquet solution decaying as x goes to $+\infty$. Differentiating (3.2) with respect to x and using the expression of K (2.8), we obtain

$$\begin{aligned}\hat{u}_x(x_R,s) &= \frac{\pi}{S_R}K\left(\frac{S_R^2(is-V_R)}{\pi^2},\frac{S_R^2 q_R}{\pi^2}\right)\hat{u}(x_R,s)\\ &= -\sqrt{-is+\tilde{a}_0^R}\prod_{r=1}^{+\infty}\frac{\sqrt{-is+\tilde{a}_r^R}}{\sqrt{-is+\tilde{b}_r^R}}\hat{u}(x_R,s),\quad \Re s>0,\end{aligned} \tag{3.3}$$

where

$$\tilde{a}_r^R = V_R+\frac{\pi^2}{S_R^2}a_r\left(\frac{S_R^2 q_R}{\pi^2}\right),\quad \tilde{b}_r^R = V_R+\frac{\pi^2}{S_R^2}b_r\left(\frac{S_R^2 q_R}{\pi^2}\right).$$

In a form of Dirichlet-to-Neumann mapping, the equation (3.3) expresses an exact absorbing boundary condition at $x=x_R$ in the transformed space. By introducing a sequence of auxiliary functions w_k^R as

$$\hat{w}_k^R(s)\overset{def}{=}\prod_{r=k}^{+\infty}\frac{\sqrt{-is+\tilde{a}_r^R}}{\sqrt{-is+\tilde{b}_r^R}}\hat{u}(x_R,s),\quad k=1,2,\cdots, \tag{3.4}$$

we rewrite the equation (3.3) into an equivalent form,

$$\begin{aligned}&\hat{u}_x(x_R,s)+\sqrt{-is+\tilde{a}_0^R}\hat{w}_1^R(s)=0,\\ &\sqrt{-is+\tilde{b}_k^R}\hat{w}_k^R=\sqrt{-is+\tilde{a}_k^R}\hat{w}_{k+1}^R,\quad k=1,2,\cdots.\end{aligned}$$

Returning to the physical space yields

$$u_x(x_R,t)+e^{-i\pi/4}e^{-i\tilde{a}_0^R t}\partial_t^{\frac{1}{2}}\left(e^{i\tilde{a}_0^R t}w_1^R(t)\right)=0, \tag{3.5}$$

$$e^{-i\tilde{b}_k^R t}\partial_t^{\frac{1}{2}}(e^{i\tilde{b}_k^R t}w_k^R)=e^{-i\tilde{a}_k^R t}\partial_t^{\frac{1}{2}}(e^{i\tilde{a}_k^R t}w_{k+1}^R),\quad k=1,2,\cdots. \tag{3.6}$$

Here $\partial_t^{\frac{1}{2}}$ denotes the half-order derivative operator defined as

$$\partial_t^{1/2}v=\frac{1}{\sqrt{\pi}}\partial_t\int_0^t\frac{v(s)}{\sqrt{t-s}}ds. \tag{3.7}$$

The readers are referred to [17] for detail.

An exact absorbing boundary condition at $x=x_L$ can be analogously derived by the above procedure. The final result reads

$$-u_x(x_L,t)+e^{-i\pi/4}e^{-i\tilde{a}_0^L t}\partial_t^{\frac{1}{2}}\left(e^{i\tilde{a}_0^L t}w_1^L(t)\right)=0, \tag{3.8}$$

$$e^{-i\tilde{b}_k^L t}\partial_t^{\frac{1}{2}}(e^{i\tilde{b}_k^L t}w_k^L)=e^{-i\tilde{a}_k^L t}\partial_t^{\frac{1}{2}}(e^{i\tilde{a}_k^L t}w_{k+1}^L),\quad k=1,2,\cdots, \tag{3.9}$$

where

$$\tilde{a}_r^L = V_L+\frac{\pi^2}{S_L^2}a_r\left(\frac{S_L^2 q_L}{\pi^2}\right),\quad \tilde{b}_r^L = V_L+\frac{\pi^2}{S_L^2}b_r\left(\frac{S_L^2 q_L}{\pi^2}\right).$$

4 Numerical issues

We consider the time discretization first. Let Δt be the time step, $t_n = n\Delta t$ the time points, and $u^n(x)$ the approximation of $u(t_n,x)$. The Crank-Nicolson scheme is a popular choice for the Schrödinger equation, which reads

$$i\frac{u^n-u^{n-1}}{\Delta t}+\frac{u^n_{xx}+u^{n-1}_{xx}}{2}=V(x)\frac{u^n+u^{n-1}}{2},\quad n=1,2,\cdots. \tag{4.1}$$

At each time step, solving the ODE (4.1) necessitates two boundary conditions at $x=x_L$ and $x=x_R$. We confine ourselves to the right boundary point, since the left one can be considered analogously. For conciseness of notation, we will omit the superscript "R" in the right boundary condition (3.5)-(3.6).

An infinite number of auxiliary functions get involved in (3.5)-(3.6), which are not realizable in the numerical implementation. Considering that K_N (see (2.9)) is a good approximation to K (see (2.8)), a natural solution to this problem is to take

$$w_k(t)=u(x_R,t),\quad \forall\, k>NR,$$

where NR is a positive integer. Since $a_r\sim r^2$ and $b_r\sim r^2$ as $r\to+\infty$, for a given tolerance ϵ we determine NR as the first integer such that

$$\frac{|a_r-b_r|}{|a_r|+|b_r|}\le\epsilon,\quad \forall r>NR.$$

Our numerical tests suggest that NR is a nondecreasing function of q, which means for larger value of $q=S_R^2q_R/\pi^2$ we need more auxiliary functions to ensure the approximating accuracy. In Table 1 we list the number of auxiliary functions for some prescribed ϵ.

Table 1: Number of auxiliary functions needed in the computation.

	$q=0.1$	$q=1$	$q=10$	$q=100$	$q=1000$
$\epsilon=10^{-6}$	3	4	8	17	46
$\epsilon=10^{-9}$	4	6	10	20	49
$\epsilon=10^{-12}$	5	7	12	22	52

Another important issue on the implementing of boundary condition (3.5)-(3.6) is the discrete approximation of the half-order derivative operator $\partial_t^{1/2}$. For any smooth function $v=v(t)$ with $v(0)=v'(0)=0$, it is known that

$$D_t^{\frac{1}{2}}v(t_n)\overset{def}{=}\sqrt{\frac{2}{\Delta t}}\sum_{m=0}^{n}\alpha_m v(t_{n-m})$$

with

$$\alpha_m=\begin{cases}\beta_k=\dfrac{(2k)!}{2^{2k}(k!)^2}, & m=2k,\\ -\beta_k, & m=2k+1\end{cases} \tag{4.2}$$

presents a second-order approximation of $\partial_t^{1/2}v(t_n)$ (see [3, 31]). By replacing $\partial_t^{1/2}$ with $D_t^{1/2}$ in (3.5)-(3.6), we derive a second-order approximation,

$$\begin{aligned}&u_x^n(x_R)+e^{-i\pi/4}e^{-i\tilde{a}_0t_n}D_t^{\frac{1}{2}}\left(e^{i\tilde{a}_0t}w_1(t)\right)(t_n)=0,\\ &e^{-i\tilde{b}_kt_n}D_t^{\frac{1}{2}}(e^{i\tilde{b}_kt}w_k)(t_n)=e^{-i\tilde{a}_kt_n}D_t^{\frac{1}{2}}(e^{i\tilde{a}_kt}w_{k+1})(t_n),\quad k=1,2,\cdots,NR.\end{aligned}$$

Or equivalently,

$$\begin{aligned}&u_x^n(x_R)+e^{-i\pi/4}\sqrt{\frac{2}{\Delta t}}\left(w_1^n-e^{-i\tilde{a}_0\Delta t}w_1^{n-1}+e^{-i\tilde{a}_0t_n}\sum_{m=2}^{n}\alpha_m\left(e^{i\tilde{a}_0t}w_1(t)\right)(t_{n-m})\right)=0,\\ &w_k^n-e^{-i\tilde{b}_k\Delta t}w_k^{n-1}+e^{-i\tilde{b}_kt_n}\sum_{m=2}^{n}\alpha_m\left(e^{i\tilde{b}_kt}w_k(t)\right)(t_{n-m})=\\ &\qquad w_{k+1}^n-e^{-i\tilde{a}_k\Delta t}w_{k+1}^{n-1}+e^{-i\tilde{a}_kt_n}\sum_{m=2}^{n}\alpha_m\left(e^{i\tilde{a}_kt}w_{k+1}(t)\right)(t_{n-m}),\quad k=1,2,\cdots,NR.\end{aligned}$$

Recalling $w_{NR+1}^n=u^n(x_R)$ we have

$$u_x^n(x_R)+e^{-i\pi/4}\sqrt{\frac{2}{\Delta t}}(u^n(x_R)+\mathrm{RES})=0, \tag{4.3}$$

where

$$\begin{aligned}\mathrm{RES}\overset{def}{=}&\sum_{k=1}^{NR+1}\left(-e^{-i\tilde{a}_{k-1}\Delta t}w_k^{n-1}+e^{-i\tilde{a}_{k-1}t_n}\sum_{m=2}^{n}\alpha_m\left(e^{i\tilde{a}_{k-1}t}w_k(t)\right)(t_{n-m})\right)\\ &-\sum_{k=1}^{NR}\left(-e^{-i\tilde{b}_k\Delta t}w_k^{n-1}+e^{-i\tilde{b}_kt_n}\sum_{m=2}^{n}\alpha_m\left(e^{i\tilde{b}_kt}w_k(t)\right)(t_{n-m})\right).\end{aligned} \tag{4.4}$$

Since RES can be computed explicitly at the n-th time step, the equation (4.3) defines a Robin-type boundary condition at $x=x_R$. The ODE problem (4.1) is then solved with any spatial discretization method. In the computation we use the standard central difference scheme. The overall scheme is thus expected to have second-order accuracy in both time and space.

At the n-th time step, we need to calculate $2\times NR+1$ discrete convolutions at the right boundary point like

$$\sum_{m=2}^{n}\alpha_m v_{n-m}. \tag{4.5}$$

When the total number of time steps is large, this operation is very costly. A fast evaluation method has been proposed in [31] for (4.5). To make this paper more self-contained, we formulate the basic idea in the following.

Suppose there exists a sum of decaying exponentials satisfying

$$\tilde{\beta}_k=\sum_{j=1}^{L}w_j e^{-s_j k},\quad s_j>0,\quad |\beta_k-\tilde{\beta}_k|\leq\epsilon,\quad k=0,1,\cdots,[N/2]. \tag{4.6}$$

Here N denotes the total number of time steps. If ϵ is small enough, it is reasonable to approximate (4.5) with

$$\sum_{m=2}^{n}\tilde{\alpha}_m v_{n-m}, \tag{4.7}$$

where

$$\tilde{\alpha}_m=\begin{cases}\tilde{\beta}_k, & m=2k,\\ -\tilde{\beta}_k, & m=2k+1.\end{cases} \tag{4.8}$$

Define

$$\mathcal{F}_{odd}(w,s;\mathbf{v},k)\overset{def}{=}\sum_{m=1}^{k}we^{-sm}v_{2k+1-2m}$$

and

$$\mathcal{F}_{even}(w,s;\mathbf{v},k)\overset{def}{=}\sum_{m=1}^{k}we^{-sm}v_{2k-2m}.$$

Thus $\mathcal{F}_{odd}(w,s;\mathbf{v},0)=\mathcal{F}_{even}(w,s;\mathbf{v},0)=0$. In addition, we have the following recursions:

$$\begin{aligned}\mathcal{F}_{odd}(w,s;\mathbf{v},k)&=e^{-s}[wv_{2k-1}+\mathcal{F}_{odd}(w,s;\mathbf{v},k-1)],\\ \mathcal{F}_{even}(w,s;\mathbf{v},k)&=e^{-s}[wv_{2k-2}+\mathcal{F}_{even}(w,s;\mathbf{v},k-1)].\end{aligned}$$

The summation (4.7) is then computed within $\mathcal{O}(L)$ operations as

$$\sum_{m=2}^{n}\tilde{\alpha}_m v_{n-m}=\begin{cases}\displaystyle\sum_{j=1}^{L}\mathcal{F}_{even}(w_j,s_j;\mathbf{v},k)-\sum_{j=1}^{L}\mathcal{F}_{odd}(w_j,s_j;\mathbf{v},k-1), & n=2k,\\ \displaystyle\sum_{j=1}^{L}\mathcal{F}_{odd}(w_j,s_j;\mathbf{v},k)-\sum_{j=1}^{L}\mathcal{F}_{even}(w_j,s_j;\mathbf{v},k), & n=2k+1.\end{cases}$$

In [31] for $N=10^6$, the authors found a sum of 81 decaying exponentials which approximates β_k with an error less than 5.0×10^{-11}. In our numerical experiments we use them to evaluate RES in (4.4).

Table 2: Parameters of the numerical tests.

Case	A	B	C	D	E	F	G
S_L	π	π	π	π	π	$\frac{\pi}{20}$	$\frac{\pi}{20}$
q_L	5	20	50	100	5	200	1000
S_R	π	π	π	π	π	$\frac{\pi}{20}$	$\frac{\pi}{20}$
q_R	5	20	50	100	100	200	1000

5 Numerical experiments

Our first numerical test is intended to demonstrating the accuracy of our absorbing boundary conditions. The potential function is $V(x)=2\cos 2x$ and the computational domain is $[x_L,x_R]=[-2\pi,2\pi]$. The initial function is $u_0=e^{-x^2+2ix}$. For comparison we compute a reference solution on $[x_L,x_R]$ by setting $NL=NR=10$ and using fairly small spatial and temporal step sizes, $h=\pi/65536$ and $\Delta t=0.0001$. Remember that NL and NR denote the number of auxiliary functions at the left and right boundary points, respectively. Fig. 7 shows the amplitude of wave function until $t=4$. In Figs. 8 and 9 we depict the relative L^2-error of the computed wave function, denoted by Err, for different spatial and temporal step sizes. It can be seen that in the regime of parameters used in our computation, our numerical scheme is second order in both space and time, if the absorbing boundary conditions are accurate enough, i.e., $NL=NR\geq 4$.

We now use our scheme to study the propagation of a Gaussian beam

$$u_0(x)=e^{-x^2+8ix},$$

under the influence of the potential function

$$V(x)=\begin{cases} 2q_L\cos\frac{2\pi(x+2\pi)}{S_L}, & x\in\left(-\infty,-2\pi+\frac{S_L}{4}\right),\\ 0, & x\in\left(-2\pi+\frac{S_L}{4},2\pi-\frac{S_R}{4}\right),\\ 2q_R\cos\frac{2\pi(x-2\pi)}{S_R}, & x\in\left(2\pi-\frac{S_R}{4},+\infty\right). \end{cases}$$

The computational domain is set as $[x_L,x_R]=[-2\pi,2\pi]$. We let $NL=NR=20$. Seven cases will be considered, of which the parameters are listed in Table 2. Figs. 10-13 show the amplitude of the computed wave function in the time interval $[0,4]$. The spatial step size is $h=\frac{4\pi}{M}=\frac{\pi}{4096}$, and the temporal step size is $\Delta t=0.001$. We can see that when the potential is weak, the Gaussian beam travels out of the computational domain without significant reflection. As the amplitude of $V(x)$ increases, more wave energy will be bounced back into the computational domain. Besides, the waves traveling in opposite direction interact with each other, and later on, some interference waves will be produced. If the periodic potential is strong enough, see Fig. 13, almost all the wave energy will be trapped in the computational domain. In Fig. 14 we depict the numerical solution

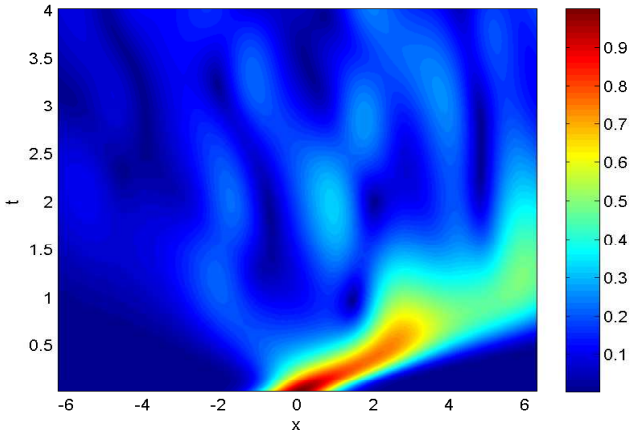

Figure 7: Amplitude of the computed wave function.

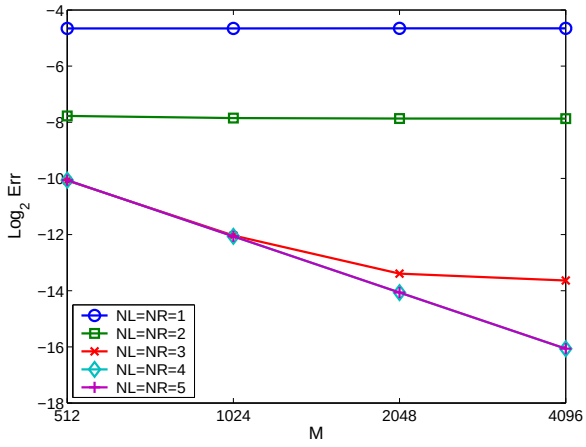

Figure 8: Error plot at the time point $t=1.6$, $\Delta t=0.0001$ with $h=\frac{4\pi}{M}$.

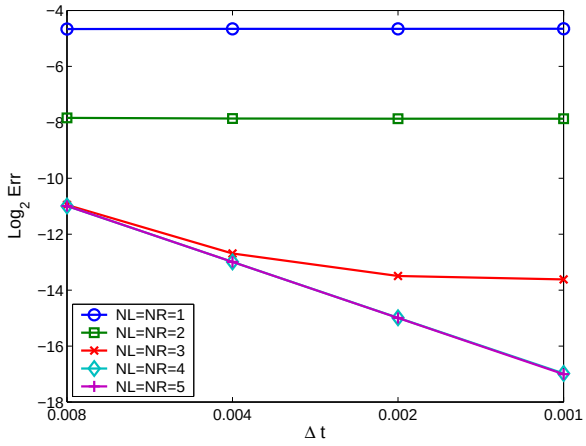

Figure 9: Error plot at the time point $t=1.6$ with $h=\frac{\pi}{65536}$.

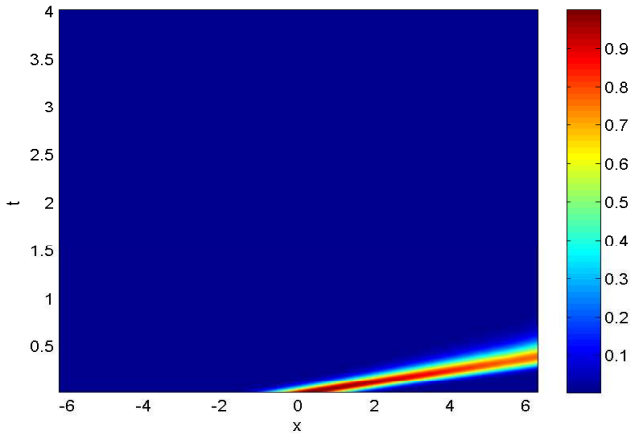

Figure 10: Amplitude of the computed wave function for case A. $h=\frac{\pi}{4096}$. $\Delta t=0.001$.

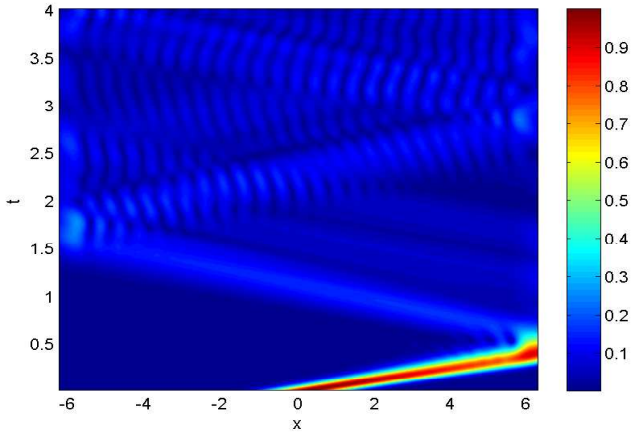

Figure 11: Amplitude of the computed wave function for case B. $h=\frac{\pi}{4096}$. $\Delta t=0.001$.

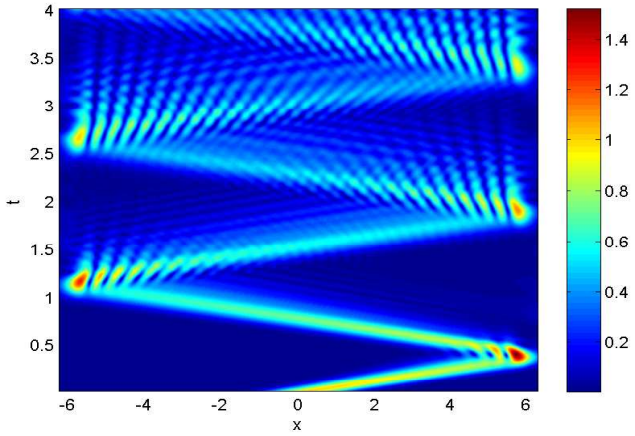

Figure 12: Amplitude of the computed wave function for case C. $h=\frac{\pi}{4096}$. $\Delta t=0.001$.

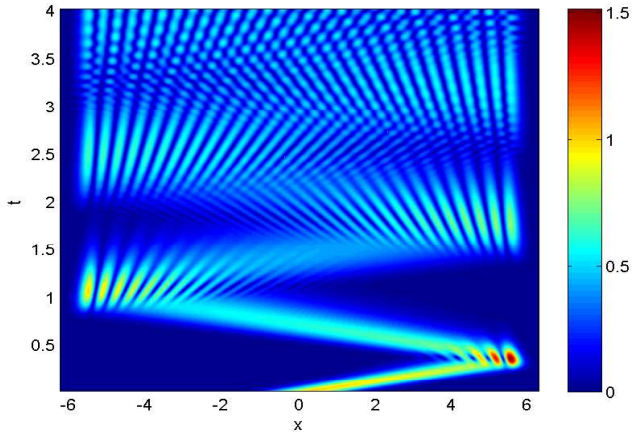

Figure 13: Amplitude of the computed wave function for case D. $h=\frac{\pi}{4096}$. $\Delta t=0.001$.

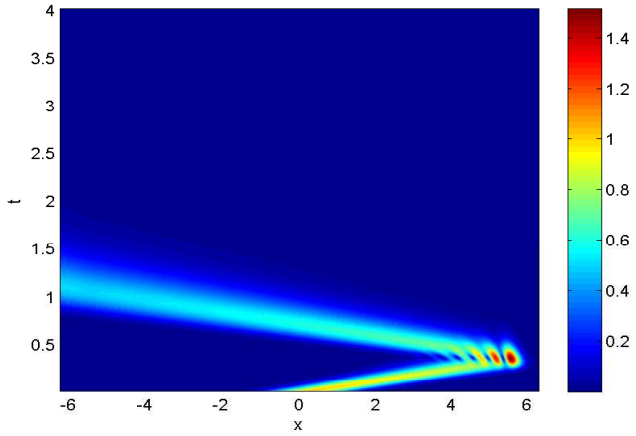

Figure 14: Amplitude of the computed wave function for case E. $h=\frac{\pi}{4096}$. $\Delta t=0.001$.

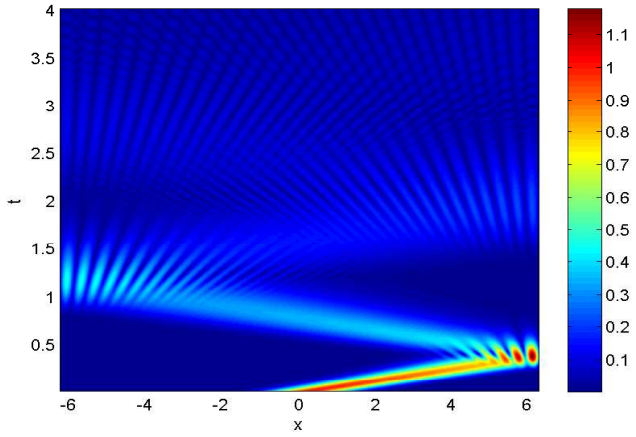

Figure 15: Amplitude of the computed wave function for case F. $h=\frac{\pi}{4096}$. $\Delta t=0.001$.

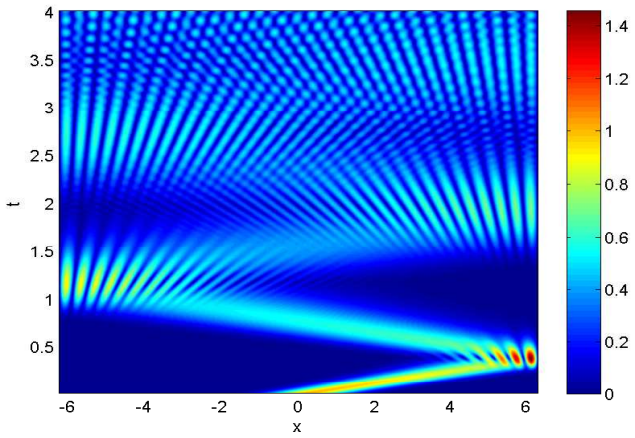

Figure 16: Amplitude of the computed wave function for case G. $h=\frac{\pi}{4096}$. $\Delta t=0.001$.

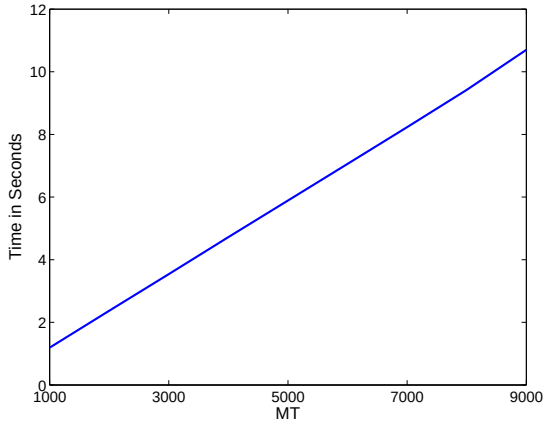

Figure 17: Computation time in seconds. $h=\frac{\pi}{1024}$. $\Delta t=\frac{4}{\mathrm{MT}}$.

when a weak potential is placed on the left of the computational domain. It can be seen that after the wave is bounced back from the first ridge of the right potential, it travels out of the computational domain through the left boundary point without obvious reflection. We also study the high energy potential with small period. For case F and case G, the wave function is shown in Figs. 15-16. Similar observations as those from Figs. 12-13 can be made.

Our last numerical experiment makes statistics on the computation cost. We consider the first numerical test, and fix the grid points to 4096. The time interval $[0,4]$ is divided into MT equidistant time steps, and we set $NL=NR=5$. In Fig. 17, we show the computation time in seconds for different MT. Our computation is performed on a PC with an Intel Core 2 Duo E6600 CPU of 2.4GHz and a memory of 3GB. It can be seen clearly that the computation time increases linearly with respect to the number of total time steps.

6 Conclusion

In this paper we have derived an exact Dirichlet-to-Neumann absorbing boundary condition for the Schrödinger equation with sinusoidal potentials at infinity. The key point of success lies in an analytical expression of the logarithmic derivative of the Floquet solution of Mathieu's equation. Our numerical tests have strongly supported the validity of this expression, though at this time we cannot prove it theoretically. Since the exact absorbing boundary condition involves an infinite product, we have simply truncated it by keeping the first several terms, thus then obtained a series of approximate boundary conditions. These boundary conditions involve the half-order time derivative operator, which is hard to compute when the number of time steps is large. To reduce the computation burden, we have applied the fast evaluation method proposed in [31]. Other kinds of methods are also applicable.

It is tempting to generalize the result in this paper to other periodic potential problems. But our first investigation on this issue suggests that the generalization might not be straightforward.

Acknowledgments

This project is supported by the National Natural Science Foundation of China under Grant No. 10401020.

References

[1] M. Abramowitz and I. A. Stegun, Handbook of Mathematical Functions with Formulas, Graphs, and Mathematical Tables, Dover, New York, 1972.
[2] I. Alonso-Mallo and N. Reguera, Discrete absorbing boundary conditions for Schrödinger-type equations. Practical implementation, Math. Comput., 73(245) (2003), 127-142.
[3] X. Antoine and C. Besse, Unconditionally stable discretization schemes of non-reflecting boundary conditions for the one-dimensional Schrödinger equation, J. Comput. Phys., 181(1) (2003), 157-175.
[4] X. Antoine, C. Besse and S. Descombes, Artificial boundary conditions for one-dimensional cubic nonlinear Schrödinger equations, SIAM J. Numer. Anal., 43(6) (2006), 2272-2293.
[5] X. Antoine, C. Besse and V. Mouysset, Numerical schemes for the simulation of the two-dimensional Schrödinger equation using non-reflecting boundary conditions, Math. Comput., 248 (2004), 1779-1799.
[6] A. Arnold, Self-consistent relaxation-time models in quantum mechanics, Commun. Part. Diff. Eq., 21 (1996), 473-506.
[7] A. Arnold and M. Ehrhardt, Discrete transparent boundary conditions for wide angle parabolic equations in underwater acoustics, J. Comput. Phys., 145 (1998), 611-638.
[8] A. Arnold, M. Ehrhardt and I. Sofronov, Discrete transparent boundary conditions for the Schrödinger equation: fast calculation, approximation, and stability, Commun. Math. Sci., 1(3) (2003), 501-556.
[9] F. M. Arscott, Periodic Differential Equations, Pergamon Press, Oxford, 1964.

[10] V. A. Baskakov and A. V. Popov, Implementation of transparent boundaries for the numerical solution of the Schrödinger equation, Wave Motion, 14 (1991), 123-128.
[11] F. Collino, Perfectly matched absorbing layers for the paraxial equations, J. Comput. Phys., 94 (1991), 1-29.
[12] P. Deuflhard and F. Schmidt, Discrete transparent boundary conditions for the numerical solution of Fresnel's equation, Comput. Math. Appl., 29(9) (1995), 53-76.
[13] T. Fevens and H. Jiang, Absorbing boundary conditions for the Schrödinger equation, SIAM J. Sci. Comput., 21 (1999), 255-282.
[14] A. S. Fokas, The generalized Dirichlet-to-Neumann map for certain nonlinear evolution PDEs, Commun. Pur. Appl. Math., 58(5) (2005), 639-670.
[15] T. Friese, F. Schmidt and D. Yevick, A comparison of transparent boundary conditions for the Fresnel equation, J. Comput. Phys., 168 (2001), 433-444.
[16] H. Galicher, Transparent boundary conditions for the one-dimensional Schrödinger equation with periodic potentials at infinity, Commun. Math. Sci., to appear.
[17] R. Gorenflo and F. Mainardi, Fractional calculus: integral and differential equations of fractional order, in: A. Carpinteri and F. Mainardi (Eds.), Fractals and Fractional Calculus in Continuum Mechanics, Springer, Wien, 1997.
[18] H. D. Han and Z. Y. Huang, Exact artificial boundary conditions for Schrödinger equation in R^2, Commun. Math. Sci., 2(1) (2004), 79-94.
[19] S. Jiang and L. Greengard, Fast evaluation of nonreflecting boundary conditions for the Schrödinger equation in one dimension, Comput. Math. Appl., 47 (2004), 955-966.
[20] C. Lubich and A. Schädle, Fast convolution for non-reflecting boundary conditions, SIAM J. Sci. Comput., 24 (2002), 161-182.
[21] B. Mayfield, Non local boundary conditions for the Schrödinger equation, Ph.D. Thesis, University of Rhodes Island, Providence, RI, 1989.
[22] J. S. Papadakis, Impedance formulation of the bottom boundary condition for the parabolic equation model in underwater acoustics, NORDA Parabolic Equation Workshop, NORDA Tech. Note 143, 1982.
[23] A. Schädle, Non-reflecting boundary conditions for the two-dimensional Schrödinger equation, Wave Motion, 35(2) (2002), 181-188.
[24] F. Schmidt and D. Yevick, Discrete transparent boundary conditions for Schrödinger-type equations, J. Comput. Phys., 134 (1997), 96-107.
[25] A. Soffer and C. Stucchio, Open boundaries for the nonlinear Schrödinger equation, J. Comput. Phys., 225(2) (2007), 1218-1232.
[26] Z. Z. Sun and X. N. Wu, The stability and convergence of a difference scheme for the Schrödinger equation on an infinite domain by using artificial boundary conditions, J. Comput. Phys., 214(1) (2006), 209-223.
[27] J. Szeftel, Absorbing boundary conditions for one-dimensional nonlinear Schrödinger equations, Numer. Math., 104 (2006), 103-127.
[28] J. Szeftel, Design of absorbing boundary conditions for Schrödinger equations in $\mathbf{R}^d$, SIAM J. Numer. Anal., 42(4) (2004), 1527-1551.
[29] Z. Xu, H. Han and X. Wu, Numerical method for the deterministic Kardar-Parisi-Zhang equation in unbounded domains, Commun. Comput. Phys., 1 (2006), 479-493.
[30] C. X. Zheng, Exact nonreflecting boundary conditions for one-dimensional cubic nonlinear Schrödinger equations, J. Comput. Phys., 215(2) (2006), 552-565.
[31] C. Zheng, Approximation, stability and fast evaluation of an exact artificial boundary condition for the one-dimensional heat equation, J. Comput. Math., to appear.